

**Li/ZnO AND CHITOSAN/Li/ZnO QUANTUM
DOTS FOR THE PHOTOCATALYTIC
OXIDATION OF OXYTETRACYCLINE**

NORMAWATI BINTI JASNI

UNIVERSITI SAINS MALAYSIA

2023

**Li/ZnO AND CHITOSAN/Li/ZnO QUANTUM
DOTS FOR THE PHOTOCATALYTIC
OXIDATION OF OXYTETRACYCLINE**

by

NORMAWATI BINTI JASNI

**Thesis submitted in fulfilment of the requirements
for the degree of
Master of Science**

April 2023

ACKNOWLEDGEMENT

In the name of Allah SWT, the entirely Gracious, the especially Merciful. All praise is due to Allah SWT for His love and guidance.

First of all, I would like to take this opportunity to thank my main supervisor, Dr Mohammad Anwar Bin Mohamed Iqbal, for accepting me to his research group, for his patience, guidance and coaching and kind help. Also, to my co-supervisor, Assoc. Professor Dr Noor Hana Hanif Binti Abu Bakar, who helped me with what was needed to complete my study. Additionally, special thanks to Dr. Wan Maryam Binti Wan Ahmad Kamil for granting access to the laboratory and research facilities. I'm grateful I had the opportunity to work with her, even for a short time.

I would like to thank my group of friends and labmates, Ms. Najahtul, Ms. Farah, Ms. Shazwani, Ms. Suma, Mrs. Aiman, Ms. Shafiqah, Ms. Hidayah, Mrs Hanisah, Ms. Najwa, Mr. Shafiq and Dr Fateemah. Every time I feel like giving up, all of you remind me how far I have come. They also make sure all my needs are well taken care of. Thank you for always being there for me and cheering me on until the end of this journey.

To my parents, my mother, Sarimah Binti Drahman, and my late father, Jasni Bin Mohamad, there is not enough thank you to express how grateful I am to have both of you. I am so glad to be your daughter. Thank you for letting me discover my potential and pushing me to my highest potential. And I would like to express my appreciation to my siblings, Azwan Bin Jasni, Norliliana Binti Omar, Norliza Binti Jasni and Azmi Bin Jasni, for your support and concern in my life. Thank you for supporting me from the beginning till where I am standing today. I cannot imagine not

having you guys as my pillars of strength. I feel blessed with you guys and this Master's was a huge achievement that I can dedicate to all of you for right now. I hope to continue to give my best and make you all proud.

Last but not least, to all staff of the School of Chemical Sciences, Centre for Global Archaeological Research, Science and Engineering Research Centre (SERC) and School of Physics, Universiti Sains Malaysia, thank you for your help and commitment. I would also like to thank the Ministry of Education Malaysia (Higher Education) for the Fundamental Research Grant Scheme (FRGS/1/2019/STG01/USM/02/7). I also want to thank myself for believing in me and doing all this hard work. I may have left out some names but know that I am not alone on this journey. Thank you, everyone.

BarakAllahu feekum!

TABLE OF CONTENTS

ACKNOWLEDGEMENT	ii
TABLE OF CONTENTS	iv
LIST OF TABLES	ix
LIST OF FIGURES	xi
LIST OF ABBREVIATIONS	xv
LIST OF SYMBOLS	xvii
LIST OF APPENDICES	xviii
ABSTRAK	xix
ABSTRACT	xxi
CHAPTER 1 INTRODUCTION	1
1.1 Overview	1
1.2 Problem statement	3
1.3 Research objectives.....	6
1.4 Scope of research	6
CHAPTER 2 LITERATURE REVIEW	8
2.1 Oxytetracycline antibiotic	8
2.2 Wastewater treatment technologies for antibiotic removal	10
2.2.1 Physical method.....	10
2.2.2 Biological method.....	11
2.2.3 Advanced oxidation processes (AOPs)	12
2.2.4 Basic mechanisms for AOPs	14
2.3 Metal oxide semiconductor as photocatalyst	16
2.4 Semiconductor nanocrystals	19

2.4.1	Physiochemical properties of QDs	20
2.4.2	Synthesis of quantum dots	25
	2.4.2(a) Solution-gelation (Sol-gel) method	26
	2.4.2(b) Microwave synthesis method	28
2.4.3	Applications of antibiotic waste-based ZnO.....	30
2.5	Surface structure modification.....	32
	2.5.1 Doping	32
	2.5.2 Surface functionalisation of ZnO QDs	35
CHAPTER 3 EXPERIMENTAL		40
3.1	Chemicals and reagents.....	40
3.2	Synthesis of Li-doped ZnO QDs.....	40
3.3	Synthesis of Chitosan/Li/ZnO QDs (CHT/Li/ZnO QDs)	41
3.4	Characterisations.....	42
	3.4.1 Fourier Transform Infrared (FT-IR) Spectroscopy.....	42
	3.4.2 Diffuse Reflectance UV-Vis Spectroscopy (UV-Vis DRS)	42
	3.4.3 Photoluminescence (PL) spectroscopy	43
	3.4.4 X-Ray Diffraction (XRD).....	44
	3.4.5 High Resolution Transmission Electron Microscope (HR-TEM).....	45
	3.4.6 Scanning Electron Microscope (SEM)	45
	3.4.7 Atomic Force Microscope (AFM)	46
	3.4.8 X-ray Photoelectron Spectroscopy (XPS)	46
	3.4.9 Thermogravimetric Analysis (TGA)	47
	3.4.10 Nitrogen Adsorption-Desorption (NAD) Analysis.....	47
	3.4.11 Photoluminescence Quantum Yield (PLQY)	48
	3.4.12 Point of Zero Charge (PZC)	49

3.4.13	Fluorescent color of quantum dots	49
3.5	Photocatalytic oxidation studies	50
3.5.1	Preparation of oxytetracycline (OTC) stock solution	50
3.5.2	Photocatalytic oxidation experimental setup	51
3.5.3	Photocatalytic oxidation activity reaction	52
3.5.4	Effect of parameters on photocatalytic oxidation activity ...	52
3.5.4(a)	Effect of the pH of the solution	53
3.5.4(b)	Effect of initial oxytetracycline concentration	53
3.5.4(c)	Effect of the photocatalyst dosage	53
3.5.5	Radical scavenging experiment	53
3.5.6	Total organic carbon (TOC) analysis	54
3.5.7	Reusability	55
CHAPTER 4 RESULTS AND DISCUSSION-CHARACTERISATION AND PHOTOCATALYTIC OXIDATION OF OXYTETRACYCLINE USING Li/ZnO QDs		56
4.1	Characterisation of Li-doped ZnO QDs (Li/ZnO QDs)	56
4.1.1	Fourier Transform Infrared (FT-IR) Spectrometer Analysis	56
4.1.2	X-Ray Diffraction (XRD) analysis	58
4.1.3	Diffuse Reflectance UV-Vis Spectroscopy analysis (UV-DRS)	62
4.1.4	High-Resolution Transmission Electron Microscope (HRTEM) analysis	65
4.1.5	Scanning Electron Microscope (SEM) analysis	67
4.1.6	Atomic Force Microscope (AFM) analysis	68
4.1.7	Photoluminescence (PL) analysis	69
4.1.8	Photoluminescence Quantum Yield (PLQY) analysis	71
4.1.9	X-Ray Photoelectron Spectroscopy (XPS) analysis	72

4.1.10	N ₂ adsorption-desorption (NAD) analysis.....	77
4.1.11	Thermogravimetric analysis (TGA)	79
4.1.12	Point of Zero Charge (PZC) analysis.....	80
4.2	Photocatalytic oxidation of oxytetracycline.....	82
4.2.1	Comparison between Li/ZnO QDs and other catalysts	82
5.2.2	Effect of pH	85
5.2.3	Effect of initial solution concentration	86
5.2.4	Effect of catalyst dosage	88
4.2.5	Radical scavenging experiment	89
4.2.6	Photocatalytic oxidation mechanism	90
4.2.7	Reusability studies	92
4.2.8	Mineralisation studies	93
4.2.9	Comparison of the Li/ZnO QDs for OTC with other photocatalysts	94
4.2.10	Summary.....	96
CHAPTER 5 RESULTS AND DISCUSSION-CHARACTERISATION AND PHOTOCATALYTIC OXIDATION OF OXYTETRACYCLINE USING CHT/Li/ZnO QDs.....		97
5.1	Characterisation of Chitosan/Li/ZnO QDs (CHT/Li/ZnO QDs)	97
5.1.1	Fourier Transform Infrared (FT-IR) Spectrometer analysis	100
5.1.2	X-Ray Diffraction (XRD) analysis	102
5.1.3	High-Resolution Transmission Electron Microscope (HRTEM) analysis.....	104
5.1.4	Scanning Electron Microscope (SEM) analysis	107
5.1.5	Atomic Force Microscope (AFM) analysis	108
5.1.6	Diffuse Reflectance UV-Vis Spectroscopy (UV-DRS) analysis	109
5.1.7	Photoluminescence (PL) analysis	111

5.1.8	Photoluminescence Quantum Yield (PLQY) analysis	112
5.1.9	X-Ray Photoelectron Spectroscopy (XPS) analysis	113
5.1.10	N ₂ adsorption-desorption (NAD) analysis	117
5.1.11	Thermogravimetric (TGA) analysis	119
5.1.12	Point of Zero Charge (PZC) analysis	121
5.2	Photocatalytic oxidation studies using Chitosan/Li/ZnO QDs (CHT/Li/ZnO QDs)	123
5.2.1	Comparison between CHT/Li/ZnO QDs and other catalysts	123
5.2.2	Effect of pH	126
5.2.3	Effect of initial solution concentration	128
5.2.4	Effect of catalyst dosage	130
5.2.5	Radical scavenging experiment	132
5.2.6	Photocatalytic oxidation mechanism	132
5.2.7	Reusability studies	134
5.2.8	Mineralisation studies	138
5.2.9	Comparison of CHT/Li/ZnO QDs with other photocatalysts	138
5.2.10	Summary	140
CHAPTER 6 CONCLUSION AND FUTURE RECOMMENDATIONS		141
6.1	Conclusion	141
6.2	Future recombination	144
REFERENCES		146
APPENDICES		
LIST OF PUBLICATIONS		

LIST OF TABLES

		Page
Table 2.1	Examples of physical adsorption methods for the removal of OTC are reported in the literature	11
Table 2.2	Examples of biological methods for the removal of OTC are reported in the literature	12
Table 2.3	List of recently reported studies on oxidation of antibiotic based on QDs.....	24
Table 2.4	List of recently reported studies on the oxidation of antibiotic based on ZnO.....	31
Table 2.5	The photocatalytic oxidation composites based on chitosan for the photocatalytic oxidation removal of organic pollutants	39
Table 4.1	The summary of XRD data for the catalyst that was prepared.	61
Table 4.2	The band gap and absorption edge values of commercial ZnO and Li/ZnO QDs	64
Table 4.3	The summary binding energy from the deconvolution and atomic concentration elements as synthesised Li/ZnO QDs	76
Table 4.4	The rate constants and correlation coefficient values of pseudo-first and pseudo-second order kinetics for the used catalyst for OTC oxidation	84
Table 4.5	The rate constants and correlation coefficient values of pseudo-first kinetics for the used catalyst for OTC oxidation on the effect of initial	86
Table 4.6	The rate constants and correlation coefficient values of pseudo-first kinetics for the used catalyst for OTC oxidation on the effect of initial concentration.....	87
Table 4.7	The rate constants and correlation coefficient values of pseudo-first kinetics for the used catalyst for OTC oxidation on the effect of dosage.....	89
Table 4.8	Comparison of photocatalytic oxidation of OTC by different photocatalysts	95
Table 5.1	The summary of XRD data for the catalyst that was prepared.	104

Table 5.2	The band gap and absorption edge values of CHT/Li/ZnO QDs	110
Table 5.3	The summary binding energy from the deconvolution as synthesised CHT/Li/ZnO QDs	115
Table 5.4	Atomic concentration elements	115
Table 5.5	Specific surface area, pore size, and pore volume as the synthesised catalysts	118
Table 5.6	The rate constants and correlation coefficient values of pseudo-first for the used catalyst for OTC oxidation	125
Table 5.7	The rate constants and correlation coefficient values of pseudo-first kinetics for the used catalyst for OTC oxidation on the effect of initial pH.....	128
Table 5.8	The rate constants and correlation coefficient values of pseudo-first kinetics for the used catalyst for OTC oxidation on the effect of initial concentration.....	130
Table 5.9	The rate constants and correlation coefficient values of pseudo-first kinetics for the used catalyst for OTC oxidation on the effect of dosage.....	131
Table 5.10	Comparison of the photocatalytic oxidation of OTC by different photocatalysts	139

LIST OF FIGURES

		Page
Figure 2.1	Different forms of the OTC antibiotic increase pH (Harja & Ciobanu, 2018)	8
Figure 2.2	A schematic represents the general photocatalytic mechanism	16
Figure 2.3	Emission and bandgap energy are based on particle size-dependent fluorescence color. Adapted from an article published by Samimi <i>et al.</i> (2017)	20
Figure 2.4	Quantum dot basic structure. Adapted from an article published by Abdel-Salam <i>et al.</i> (2020).....	37
Figure 2.5	The chemical structure of chitosan	38
Figure 3.1	Image of ZnO QDs under UV 365 nm UV lamp.....	50
Figure 3.2	Digital image of a handmade photo-reactor	51
Figure 4.1	FTIR spectra of (a) 0.05MLi/ZnO QDs, (b) 0.1MLi/ZnO QDs and (c) commercial ZnO.....	58
Figure 4.2	XRD patterns of commercial ZnO compared with Li/ZnO QDs as synthesised	59
Figure 4.3	Unit cell of wurtzite structure	62
Figure 4.4	(a) UV-Vis diffuse reflectance spectrum as-prepared photocatalyst, and (b) estimated energy gap	64
Figure 4.5	TEM images of (a) commercial ZnO, (b) 0.05MLi/ZnO QDs, (c) 0.1MLi/ZnO QDs. The particle size distribution image of (d) 0.05MLi/ZnO QDs, (e) 0.1MLi/ZnO QDs. HRTEM image of (f) 0.05MLi/ZnO QDs, (g) 0.1MLi/ZnO QDs	66
Figure 4.6	SEM images of the (a) commercial ZnO, (b) 0.05MLi/ZnO QDs and (c) 0.1MLi/ZnO QDs.....	68

Figure 4.7	Topographic AFM of the (a) 0.05MLi/ZnO QDs and (b) 0.1MLi/ZnO QDs	69
Figure 4.8	(a) Photoluminescence spectra. Deconvoluted spectra of (b) 0.05MLi/ZnO QDs and (c) 0.1MLi/ZnO QDs	71
Figure 4.9	Fluorescence quantum yield of the prepared photocatalyst.....	72
Figure 4.10	(a) The XPS general scans and the deconvolution XPS spectra in (b) Zn 2p, (c) Li 1s, and (d) O 1s	75
Figure 4.11	The N ₂ adsorption-desorption isotherms of (a) 0.05MLi/ZnO QDs, and (b) 0.1MLi/ZnO QDs. Inset: The BJH pore size distribution.....	78
Figure 4.12	TGA (a) 0.05MLi/ZnO QDs, (b) 0.1MLi/ZnO QDs and (c) the stability of Li/ZnO QDs.....	80
Figure 4.13	The pHPZC of (a) 0.05MLi/ZnO QDs and (b) 0.1MLi/ZnO QDs	81
Figure 4.14	(a) Removal efficiency of OTC using different catalyst (OTC = 10 mg L ⁻¹ , catalyst dosage = 10 mg, pH = 9, fluorescent irradiation). Kinetic curve for evaluating the rate constant (k) (b) pseudo-first order and (c) pseudo-second order	84
Figure 4.15	(a) Removal efficiency of OTC at different initial pH and (b) the kinetic curve to evaluate the rate constant (k)	86
Figure 4.16	(a) Removal efficiency of OTC at different initial concentration and (b) the kinetic curve to evaluate the rate constant (k)	87
Figure 4.17	(a) Removal efficiency of OTC at different initial dosage and (b) kinetic curve to evaluating the rate constant (k).....	89
Figure 4.18	The free radical trapping experiment.....	90
Figure 4.19	Schematic of the charge transfer in the 0.1MLi/ZnO QDs.....	91
Figure 4.20	(a) Reusability of photocatalytic oxidation of OTC in presence of 0.1MLi/ZnO QDs, (b) XRD and (c) FTIR spectra of the	

	0.1M Li/ZnO QDs catalyst before and after photocatalytic oxidation of OTC for 5 runs	93
Figure 5.1	Diagram of the formation of Li/ZnO QDs.....	99
Figure 5.2	CHT/Li/ZnO QDs presented in a simplified form. Adapted from article by Bashal <i>et al.</i> (2020).....	99
Figure 5.16	FTIR spectra of (a) Li/ZnO QDs, (b) 0.5% CHT/Li/ZnO QDs, (c) 1.0% CHT/Li/ZnO QDs, and (d) CHT	102
Figure 5.4	XRD patterns of (a) Li/ZnO QDs, (b) 0.5% CHT/Li/ZnO QDs, and (c) 1.0% CHT/Li/ZnO QDs.....	104
Figure 5.5	TEM images with corresponding particles size distributions of (a, b) 0.5% CHT/Li/ZnO QDs, (c, d) 1.0% CHT/Li/ZnO QDs. HRTEM image (e) 0.5% CHT/Li/ZnO QDs and (f) 1.0% CHT/Li/ZnO QDs.....	106
Figure 5.6	SEM images of the (a) 0.5% CHT/Li/ZnO QDs, and (b) 1.0% CHT/Li/ZnO QDs.....	108
Figure 5.7	Topographic AFM of the (a) 0.5% CHT/Li/ZnO QDs and (b) 1.0% CHT/Li/ZnO QDs	109
Figure 5.8	(a) UV-Vis diffuse reflectance spectrum of the as-prepared photocatalyst, and (b) estimated energy gap	110
Figure 5.9	(a) Photoluminescence spectra. Deconvoluted spectra of (b) 0.5% CHT/Li/ZnO QDs and (c) 1.0% CHT/Li/ZnO QDs	112
Figure 5.10	Fluorescence quantum yield of the as prepared photocatalyst .	113
Figure 5.11	(a) The XPS general scans and the deconvolution XPS spectra in (b) Zn 2p, (c) O 1s, (d) Li 1s and (e) C 1s.....	116
Figure 5.12	The N ₂ adsorption-desorption isotherm of (a) 0.5% CHT/Li/ZnO QDs, and (b) 1.0% CHT/Li/ZnO QDs. Insert: BJH pore size distribution	119
Figure 5.13	TGA (a) 0.5% CHT/Li/ZnO QDs, (b) 1.0% CHT/Li/ZnO QDs and (c) comparison between Li/ZnO QDs and CHT/Li/ZnO QDs.....	121
Figure 5.14	The pHPZC of (a) 0.5% CHT/Li/ZnO QDs and (b) 1.0% CHT/Li/ZnO QDs.....	122
Figure 5.15	(a) Removal efficiency of OTC using different catalyst (OTC = 10 mg L ⁻¹ , catalyst dosage = 10 mg, pH = 9, fluorescent	

	irradiation), and (b) the kinetic curve to evaluate the rate constant (k) for pseudo first order	125
Figure 5.16	(a) Removal efficiency of OTC at different initial pH and (b) the kinetic curve to evaluate the rate constant (k)	128
Figure 5.17	(a) Removal efficiency of OTC at different initial concentrations, and (b) the kinetic curve to evaluate the rate constant (k)	129
Figure 5.18	(a) Removal efficiency of OTC at different initial dosages and (b) the kinetic curve to evaluate the rate constant (k)	131
Figure 5.19	The free radical trapping experiment.....	132
Figure 5.20	Schematic of the charge transfer in the 1.0% CHT/Li/ZnO QDs.	134
Figure 5.21	(a) Reuseability of photocatalytic oxidation of OTC in presence of 1.0% CHT/Li/ZnO QDs, (b) XRD and (c) FTIR spectra of the 1.0% CHT/Li/ZnO QDs catalyst before and after photocatalytic oxidation of OTC for 5 runs	136
Figure 5.22	TOC removal performance between the Li/ZnO QDs and CHT/Li/ZnO QDs.....	137

LIST OF ABBREVIATIONS

BET	Brunauer-Emmet-Teller
BJH	Barett Joyner and Halenda
CB	Conductive Band
DRS	Diffuse Reflectance spectroscopy
ICP OES	Inductive coupled plasma atomic emission spectroscopy
UV	Ultraviolet
VB	Valence band
LiOH	Lithium hydroxide
<i>hkl</i>	Miller indices
PZC	Point of zero charge
QDs	Quantum Dots
TOC	Total organic carbon
Vis	Visible
$h\nu$	The energy of a photon
AA	Ascorbic acid
AFM	Atomic Force Microscope
AOPs	Advanced Oxidation Process
SEM	Scanning electron microscopy
FT-IR	Fourier transform infrared
HRTEM	High resolution transmission electron microscopy
PL	Photoluminescence
QCE	Quantum confinement effect
OTC	Oxytetracycline
TGA	Thermogravimetric
XPS	X-ray photoelectron spectroscopy

XRD	X-ray diffraction
ZnO	Zinc Oxide
IPA	Isopropanol
EDTA	Ethylenediaminetetraacetic acid
mL	Mili-liter
ROS	Reactive oxygen species
NPs	Nanoparticles
ARGs	antibiotic resistance genes
WHO	World Health Organization
AMR	antimicrobial resistance
eV	Electronvolt
US FDA	United States Food and Drug Administration
GRAS	Generally Recognized As Safe
W	Watts
ZnO	Zinc oxide
PLQY	Photoluminescence quantum yield
CHT	Chitosan
NHE	Normal hydrogen electrode
Rq	Root mean square roughness
BE	Binding energy
IUPAC	International Union of Pure and Applied Chemistry
NIST	The National Institute of Standards and Technology

LIST OF SYMBOLS

e^-	Electrons
k'	Pseudo-first-order rate constant
k''	Pseudo-second-order rate constant
OH^-	Hydroxyl ion
h^+	Positive holes
$\cdot\text{O}_2^-$	Superoxide radical
$\cdot\text{OH}$	Hydroxyl radical
H^+	Proton
V_{Zn}	Zinc vacancy
V_{Zni}	Zinc interstitial
O_v	Oxygen vacancy
O_i	Oxygen interstitial
$\text{V}_{\text{O}^{++}}$	Doubly charged oxygen vacancy
V_{O^+}	Singly charged oxygen vacancy
0D	Zero-dimensional
1D	One-dimensional
2D	Two-dimensional
3D	Three-dimensional
E_g	Band gap

LISTS OF APPENDICES

- Appendix A Physical and fluorescent colour changes after fifth run of reusability
- Appendix B Changes in the spectrum of OTC using (a) 0.1M Li/ZnO QDs and (b) 1.0% CHT/ZnO QDs with the passage of time

Li/ZnO DAN KITOSAN/Li/ZnO TITIK KUANTUM UNTUK FOTOPEMANGKINAN OKSIDASI OKSITETRASIKLIN

ABSTRAK

Titik kuantum adalah satu kelas bahan bersaiz nano yang berpotensi untuk dimajukan sebagai fotopemangkin berdasarkan keupayaannya menyerap cahaya nampak, menjana berbilang pengujaan akibat kurungan kuantum, mempunyai sifat bercahaya dan nisbah permukaan ke isipadu yang tinggi. Kajian ini dibahagikan kepada dua bahagian. Dalam bahagian pertama, ZnO titik kuantum disintesis melalui kaedah gelombang mikro dengan menggunakan Li^+ sebagai agen penutup (Li/ZnO QDs). Dalam bahagian kedua, Li/ZnO QDs diubahsuai dengan mengkapsul Li/ZnO QDs (CHT/ Li/ZnO QDs) dengan kitosan untuk meningkatkan sifat fizikokimia Li/ZnO QDs. Fotopemangkin yang disintesis dicirikan dengan spectrometer transformasi fourier inframerah (FTIR), belauan sinar-X (XRD), mikroskop elektron penghantaran resolusi tinggi (HRTEM), mikroskop elektron pengimbasan (SEM), spektroskopi kepantulan baur UV-vis (UV-DRS), fotoluminasi (PL), daya atom mikroskop (AFM), spektroskopi fotoelektron sinar-X (XPS) dan analisis termogravimetri (TGA). Analisis SEM menunjukkan bahawa penambahan kitosan telah menghalang Li/ZnO QDs daripada aglomerasi. Analisis AFM mengukur kekasaran permukaan Li/ZnO QDs dan CHT/ Li/ZnO QDs sebagai 21.7 to 33.2 nm, masing-masing. Peningkatan disebabkan kebolehan kitosan membentuk bijian kecil yang kurang padat. Analisis XRD menunjukkan bahawa kedua fotopemangkin mempunyai struktur kristal jenis wurtzite. Peningkatan nisbah molar Li^+ dalam Li/ZnO QDs menyebabkan pengurangan kehabluran dan saiz zarah akibat penggantian Zn^{2+} oleh Li^+ dalam kekisi ZnO, menyebabkan kewujudan spesis [$\text{Li}^+ \text{O}^-$] cacat. Penambahan

kitosan seterusnya mengurangkan saiz dari 10.0 ± 0.39 nm ke 7.86 ± 0.28 nm. Pengurangan saiz hablur dan saiz partikel telah meningkatkan jurang jalur fotopemangkin (E_g). E_g yang dianggarkan dari analisis PL adalah 3.21 ke 3.30 eV. Analisis NAD menunjukkan luas permukaan Li/ZnO QDs dan CHT/Li/ZnO QDs adalah $47.54 - 39.48$ m²/g dan $31.88 - 42.80$ m²/g dengan taburan saiz liang (BJH) bagi adalah diantara 13.56 - 9.1 nm. Li⁺ yang dimaksudkan bertindak sebagai penerima elektron yang menggalakan pengasingan elektron dan lubang (h⁺) fotopenjanaan secara efisien selain menjadi agen penutup. Penambahan kitosan tidak menambahbaik peratus penyingkiran OTC tetapi kumpulan NH₂ dan sifat hidrofilik membantu ampai dan menolak satu sama lain melalui daya columbic dan halangan sterik. Selain itu, pengkapsulan Li/ZnO QDs dengan chitosan boleh mengubah keadaan pH daripada berasid kepada alkali, yang merupakan pH yang sesuai dalam rawatan air buangan. Tambahan pula, keadaan pH yang berubah-ubah ini disebabkan oleh chitosan sebagai polisakarida alkali dan hidrolarut dalam keadaan berasid. Kecekapan penyingkiran OTC menggunakan Li/ZnO QDs adalah 94.7%. manakala CHT/Li/ZnO QDs menyingkirkan 97.4%. Keadaan optimum bagi Li/ZnO QDs adalah [OTC] = 10 mg L⁻¹, dos fotopemangkin = 0.01 g pada pH = 5 manakala bagi CHT/Li/ZnO QDs adalah [OTC] = 10 mg L⁻¹, dos fotopemangkin = 200 mg L⁻¹ pada pH = 9. Kedua-dua fotopemangkin menghasilkan h⁺ and $\cdot O_2^-$ yang bertanggung dalam proses pengoksidaan fotopemangkin. $\cdot OH$, sebaliknya disokong bersama untuk tindak balas. Fotopemangkin dapat digunakan sebanyak lima kali tanpa kehilangan potensi. Keputusan menunjukkan bahawa kesan saiz nano untuk kedua-dua Li / ZnO QDs dan CHT/Li/ZnO QDs berfungsi sebagai pemangkin yang cekap untuk pengoksidaan OTC merentasi pelbagai sifat penyerapan cahaya, walaupun dengan dos pemangkin rendah dan eksperimen kos rendah.

Li/ZnO AND CHITOSAN/Li/ZnO QUANTUM DOTS FOR THE PHOTOCATALYTIC OXIDATION OF OXYTETRACYCLINE

ABSTRACT

Quantum dots are a class of nano-sized materials that have the potential to be developed into photocatalysts due to their ability to absorb visible light, generate multiple excitons due to quantum confinement, have luminescent properties, and have a high surface-to-volume ratio. This study is divided into two parts. In the first part, Li/ZnO quantum dots (Li/ZnO QDs) was synthesized via microwave methods utilizing Li^+ ion as capping agent. In the second part, the Li/ZnO QDs were encapsulated with chitosan (CHT/Li/ZnO QDs) to enhance the physicochemical properties of Li/ZnO QDs. The synthesised photocatalyst were characterised using Fourier-transform infrared (FT-IR) spectrometer, x-ray diffraction (XRD), high-resolution transmission electron microscope (HRTEM), scanning electron microscope (SEM), UV-vis diffuse reflectance spectroscopy (UV-DRS), photoluminescence (PL), nitrogen adsorption-desorption analysis (NAD) analysis, atomic force microscopy (AFM), x-ray photoelectron spectroscopy (XPS) and thermal stability (TGA). The SEM analysis shows that adding chitosan prevented the Li/ZnO QDs from agglomerating. The AFM analysis measured the surface roughness of Li/ZnO QDs and CHT/Li/ZnO QDs to be 21.7 to 33.2 nm, respectively. The increase is due to the ability of chitosan to form loosely packed smaller grains. The XRD analysis indicates that both photocatalysts contains hexagonal wurtzite type crystal structure. Increasing Li molar ratio in Li/ZnO QDs, resulted in the reduction of crystallite and particle size due to substitution of Zn^{2+} by Li^+ in the ZnO lattice, lead to the formation of defect [$\text{Li}^+ \text{O}^-$] species. The addition of chitosan further reduced the size to 10.0 ± 0.39 nm to 7.86 ± 0.28 nm. The reduction

in crystallize and particle size increase the band gap energy (E_g). The E_g estimated from PL analysis were 3.21 to 3.30 eV. The NAD analysis determined the surface area of Li/ZnO QDs to be 47.54 - 39.48 m^2/g whereas the CHT/Li/ZnO QDs was 31.88 - 42.80 m^2/g with both study sections having a (BJH) pore size of around 13.45 - 9.1 nm. The incorporated Li^+ ions act as electron acceptor that will promote the efficient separation of the photogenerated electron and holes in addition of being a capping agent. The addition of chitosan did not improve the removal percentage of OTC, but the presence of NH_2 groups and the hydrophilic properties of chitosan assisted the aqueous phase catalysts to improve their suspension and cause them to oppose one another through columbic force and steric hindrance. Additionally, the encapsulation of Li/ZnO QDs with chitosan can change the pH condition from acidic to alkaline, which is a favorable pH in wastewater treatment. Furthermore, this changing pH condition due to chitosan being an alkaline polysaccharide and hydrosoluble in acidic condition. The removal efficiency of OTC using Li/ZnO QDs was 94.7%. Whereas CHT/Li/ZnO QDs was achieved 97.4%. The optimum conditions for the removal of OTC using Li/ZnO QDs were $[OTC] = 10 \text{ mg L}^{-1}$, photocatalyst dosage = 200 mg L^{-1} at $pH = 5$. Whereas for CHT/Li/ZnO QDs the conditions were $[OTC] = 10 \text{ mg L}^{-1}$, photocatalyst dosage = 0.01 g at $pH = 9$. Both photocatalysts generated h^+ and $\cdot O_2^-$ that were responsible for the photocatalytic oxidation. $\cdot OH$, on the other hand, is co-supported for the reaction. The photocatalysts were able to be recycled for five times without losing its potential. The results showed that the nano-size effect for both Li/ZnO QDs and CHT/Li/ZnO QDs served as efficient catalysts for OTC oxidation across a wide range of light absorption properties, even with low catalyst dosages and low-cost experiments.

CHAPTER 1

INTRODUCTION

1.1 Overview

It is estimated that almost 200,000 metric tonnes of antibiotics are used to treat various infectious diseases in humans and animals (Guo *et al.*, 2022; Hom-Diaz *et al.*, 2022). In the aquatic environment, it can generate antibiotic resistance genes (ARGs) in microorganisms. Murray *et al.* (2022) reported that the number of deaths caused by antimicrobial resistance (AMR) infection in 2019 was 4.95 million. *Escherichia coli*, *Staphylococcus aureus*, *Klebsiella pneumoniae*, *Streptococcus pneumoniae*, *Acinetobacter baumannii*, and *Pseudomonas aeruginosa* were identified as the leading pathogens (Murray *et al.*, 2022; Moghni *et al.*, 2022). The World Health Organization (WHO) estimated that bacterial antimicrobial resistance would cause up to 10 million deaths by 2050 (Murray *et al.*, 2022). Antimicrobial resistance will continue to spread and escalate if no actions are taken to curb it. Besides, the health inequities and the high cost of treating antimicrobial-resistant infections will worsen these infections in low- and middle-income countries (Kusi *et al.*, 2022). Since there have been a lot of hospitalisations from the COVID-19 pandemic and now influenza between 2019 and 2022, there is a chance that the burden of antimicrobial resistance has already escalated due to increased antibiotic use (Kariyawasam *et al.*, 2022). Antibiotic resistance among microbial species is found to be very high due to the ongoing release of antibiotics into the aquatic environment (Paul *et al.*, 2007). There is evidence that the oxidation byproducts are even more hazardous than the parent substances (Zhao *et al.*, 2010).

Among the antibiotics present, tetracycline is a popular antibiotic that is used to treat illness in both people and animals (Yang *et al.*, 2017). Because of their widespread use around the world, four tetracycline antibiotics, oxytetracycline (OTC), tetracycline (TC), chlortetracycline (CTC), and doxycycline (DTC), are regularly found in surface water and wastewaters (Chan *et al.*, 2022). In addition, OTC is one of the most commonly used antibiotics in the aquaculture, livestock, and feeding industries because it is a typical broad-spectrum, effective, and affordable antibiotic (Huang *et al.*, 2020). However, due to OTC's long-term stability due to its solid ring structure and low biodegradability, conventional water treatment techniques like physiochemical or biological treatment are ineffective for eradicating it (Liu *et al.*, 2023; Park *et al.*, 2023). As a result, this antibiotic is frequently found in surface waters and poses a huge threat to human health.

Advanced oxidation processes (AOPs) are techniques for eliminating organic pollutants from aqueous solutions that rely on the production of highly reactive species with high oxidation capacities and rapid mineralisation of pollutants (Lai *et al.*, 2023). In order to degrade the organic compounds found in wastewater, photocatalysis from AOPs is used. It is a simple, affordable, and environmentally friendly energy method (Ren *et al.*, 2021). ZnO stands out as a potential semiconductor due to its increased quantum efficiency for superior photocatalytic performance, capability, affordability, and environmental friendliness (Chai *et al.*, 2023). However, because they have a large band gap of 3.37 eV, their photocatalytic activity is limited under visible light, and their high exciton binding energy causes their photo-generated charge carriers to combine quickly (Hunge *et al.*, 2023).

To overcome these drawbacks, ZnO quantum dots (QDs) are considered an ideal photocatalyst because the quantum confinement effect produces fascinating

optical characteristics. For example, the higher the catalytic reaction surface, the wider the band gap, and the better the photocatalytic performance of ZnO QDs, which result from being smaller semiconductor particles (Tayyebi *et al.*, 2016). However, due to their smaller size, QDs have high surface energy, which leads to aggregation and uncontrolled growth. Aggregation reduces surface area and the capacity for photocatalytic degradation (Banerjee & Kar 2023). Thus, QDs must be immobilised to be used in outstanding practical applications (Janbandhu *et al.*, 2023). Potentially, chitosan encapsulation of ZnO QDs could be a useful strategy (Shu *et al.*, 2023). The nontoxic and biodegradable properties of biopolymer-functioned ZnO have gained interest in the biomedical and pharmaceutical industries (Preethi *et al.*, 2020). Also, because it is environmentally friendly, antibacterial, and non-mutagenic, chitosan has attracted a lot of attention (Asgari-Targhi *et al.*, 2021; Preethi *et al.*, 2020; Gasti *et al.*, 2022).

In this study, the performances of Li/ZnO QDs and CHT/Li/ZnO QDs as photocatalysts in the photocatalytic oxidation of OTC under fluorescent light are synthesised using the microwave method. Additionally, the microwave method is an economical, fast synthesis and can expand creativity to develop the smaller QDs' seeds. Then, their performance in oxidation will be compared with commercial ZnO and TiO₂ (Degussa P25) and further with photocatalysts available in the literature.

1.2 Problem statement

ZnO is a potential photocatalyst due to its affordability (Sanakousar *et al.*, 2022), non-toxicity, and being considered a 'GRAS' substance by the US FDA (Sathish *et al.*, 2021), which makes it more advantageous than other semiconductors. Despite its versatility, ZnO as a photocatalyst only utilises a limited portion of the solar

beam (UV-light region, 3-5%) that reaches the earth because of its wide band gap (3.37 eV), which hinders the absorption of visible light. In addition, photoinduced charge carriers quickly recombine, preventing them from reaching the surface and delaying chemical reactions at the semiconductor/liquid interface, reducing the photocatalytic oxidation process's efficiencies.

Quantum dots have been synthesised using both top-down and bottom-up methods. However, top-down processes like laser ablation, arc discharge, and chemical etching typically require several phases that involve concentrated acids, strong oxidising agents, and high temperatures. The main problem with this method is the difficulty in managing the shape and size distribution of QDs. In contrast, bottom-up approaches create QDs by utilising atomic or molecular precursors. Higher atomic utilisation, better structural control, and the ability to control size and morphology are intriguing benefits of this approach (Manikandan *et al.*, 2019). Microwave synthesis, a bottom-up technique, has lived up to its promise of being quick and simple while also being inexpensive. This allows for higher yield, lower impurity levels, size and temperature control, as well as improved safety, reproducibility, and excellent control over experimental parameters (Singh *et al.*, 2019).

According to Li *et al.* (2016), a common technique for making ZnO QDs comprises the basic hydrolysis of zinc acetate under the control of an alkali metal hydroxide in an alcoholic solvent. Some studies have been conducted on doped-ZnO with transition metals, alkali earth metals, and rare earth metal, resulting in larger crystallite size, distortion of lattice structure due to a larger ionic radius, and a tendency to easily agglomerate. Thus, lithium results from I-group elements, which were chosen due to lithium's acceptor-donor behavior when substituting Zn sites as their ionic radius is closer to each other. A larger electronegativity makes it easier for Li⁺ ions to

be attracted to the negatively charged ZnO QDs surface, and a smaller ionic radius makes it possible for Li^+ ions to form a more compact passivation layer. On the other hand, the smaller ZnO QDs can only be produced when Li cations co-exist with excessive OH^- anion (Li *et al.*, 2016). Encapsulation is now widely used in the synthesis of nanoparticles because the concentration of the encapsulation molecules can control the particle size as well as protect it from coagulation since most applications are in suspension. Additionally, the introduction of new photophysical and photochemical properties resulting from combinatorial effects is also made possible by the use of encapsulation (Vidhya *et al.*, 2015). Because of the hydrophilicity and cationic charge of chitosan, encapsulating NPs with one amino and two hydroxyl groups of chitosan might increase their stability in aqueous media (Yuan *et al.*, 2010).

The OTC is well known to induce microbial resistance. Furthermore, the current existing sewage treatment technologies are insufficient to remove OTC from wastewater efficiently. The complexity of the traditional process and the high cost limit their use. Photocatalysis has the advantage of quickly oxidising contaminants into harmless by-products, which makes it possible to eradicate many different pollutants.

1.3 Research objectives

The objectives of this research are:

1. To synthesise the Li/ZnO QDs and CHT/Li/ZnO QDs photocatalyst, via microwave method.
2. To characterise the photocatalyst, using various spectroscopic and microscopic techniques.
3. To compare the performance of Li/ZnO QDs and CHT/Li/ZnO QDs with commercially available ZnO and TiO₂ (Degussa P25) in the photocatalytic oxidation of OTC under fluorescent light and mechanism as a photocatalyst.

1.4 Scope of research

This study is intended to investigate the potential of Li ions and chitosan as doping and encapsulation agents in the synthesis of ZnO QDs via the microwave synthesis method. Li ions were chosen due to their growing ability to act as electron acceptors, induce defects, and reduce particle size. Chitosan is a biocompatible polymer that can control the particle size and crystalline phase, prevent particle aggregation, and introduce more functional groups to the ZnO QDs.

This thesis is divided to five chapters:

Chapter 1 is an overview of the study. The problem statement and content overview are highlighted. It also includes a thorough literature review on some fundamental concepts, such as the presence and effect of antibiotics, mainly OTC, the most effective type of wastewater treatment technology, and semiconductor quantum dots' properties.

Chapter 2 details the materials and methodology used for this study. The characterisation methods via various microscopic and spectroscopic were discussed.

Lastly, the experimental procedures employed by the photocatalytic oxidation was described.

Chapter 3 and 4 discussed the detailed characterisation of the synthesis Li/ZnO QDs. and CHT/Li/ZnO QDs. Also, discussion on the photocatalytic oxidation of OTC using the photocatalysts was discussed.

Chapter 5 presents the study's conclusion and provides recommendations for future work.

CHAPTER 2

LITERATURE REVIEW

2.1 Oxytetracycline antibiotic

Oxytetracycline (OTC) is a persistent organic pollutant that belongs to the antibiotic tetracycline class (Nguyen *et al.*, 2022; Pelosato *et al.*, 2022). They have similar structures but differ in the number and placement of hydroxyl groups (Xu *et al.*, 2022). According to Zhang *et al.* (2022), the absorption band centred at 355 and 276 nm were observed in the primary structure of OTC, which was derived from the chromophores group of the naphthol ring. The absorption peak at 355 nm indicates that the phenolic group (B, C, and D) has linked itself to the aromatic ring. At 276 nm, the enolic hydroxyl and amide groups of OTC are responsible (Chen & Huang, 2011; Kandi *et al.*, 2020). Four types of OTC, each with a unique electric charge state and a variety of pH values, are depicted in Figure 2.1. OTC is nearly entirely protonated (H_3OTC^+) at pH levels lower than 3. When the pH ranges from 4 to 7, the majority of zwitterion form (H_2OTC^\pm) by shedding the tricarbonyl group. Then, the OTC above pH 9 is mostly represented for the proportion of $HOTC^-$, but at pH 11, the OTC is primarily represented by OTC^{2-} (Zhao *et al.*, 2013).

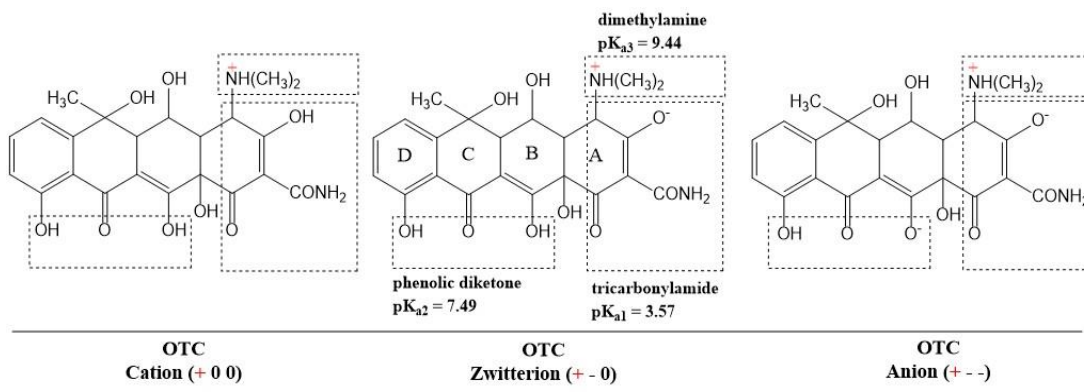


Figure 2.1: Different forms of the OTC antibiotic increase pH (Harja & Ciobanu, 2018).

Due to its affordability, good quality, and potent therapeutic impact, OTC is frequently used to treat a variety of disorders, such as human pneumonia, coryza infection, chicken cholera, bacterial disease management in fruits and cattle growth promotion (Pokrant *et al.*, 2021; Majumdar & Pal, 2020; Gusain *et al.*, 2021). Both humans and animals can partially absorb and digest OTC, and more than half (up to 75%) (Karpov *et al.*, 2018) of it is expelled through the digestive system, leaving significant OTC residues in the environment (Ma *et al.*, 2022) including through drainage from agricultural land (Pelosato *et al.*, 2022). Its residues have been found in water and soil (Li *et al.*, 2021). The concentrations of OTC antibiotics in China have been observed to be between 0.16 and 5.7 $\mu\text{g L}^{-1}$ (Di *et al.*, 2020). Choi *et al.* (2020) found that concentrations of OTC in natural water systems were 116 ng L^{-1} . Also, Andriamanohiarisoamanana *et al.* (2020) reported that OTC concentrations of 40 to 1240 mg L^{-1} in dairy manure.

The OTC is highly stable and unable to degrade by itself due to its polyaromatic ring structure (Wu *et al.*, 2022). Therefore, its presence in bodies of water for a longer period will generate antibiotic resistance genes between environmental bacteria and human pathogens, weakening the therapeutic effect of antibiotics (Ma *et al.*, 2022) and posing serious health by increasing the risk of cancer, cardiovascular disease, affecting cell growth, and suppressing the activity of the human gut microbiota (Martins *et al.*, 2014; Magdaleno *et al.*, 2015; Francino, 2016). Thus, the OTC can be classified as carcinogenic, mutagenic, and endocrine disrupting (Chen *et al.*, 2014).

2.2 Wastewater treatment technologies for antibiotic removal

The extensive use of antibiotics, particularly antibiotic misuse and abuse, has caused public concern. Antibiotic removal techniques are currently classified into three wastewater treatment methods: physical, biological, and advanced oxidation process (AOPs). Alternative and efficient wastewater treatment technologies have risen in demand due to rising economic, energy, and environmental pressures to eliminate OTC from the aquatic environment.

2.2.1 Physical method

Physical treatment usually involves separating contaminants from the aquaculture wastewater in their original form of contaminant without degrading desired substances into by-products (Ahmad *et al.*, 2022). Adsorption, membrane, and conventional coagulation are examples of common physical methods (Breazeal *et al.*, 2013; Sanakousar *et al.*, 2022). The process of attracting and accumulating contaminants onto an adsorbents' surface is known as adsorption (Kamarudin *et al.*, 2021). Membrane contains small pores, and solutes bigger than these pores would be trapped behind them when wastewater passes through the membrane (Kamarudin *et al.*, 2021). Even though membranes have to be replaced frequently, they are relatively expensive (Sun *et al.*, 2022). Whereas coagulation-sedimentation methods based on the coprecipitation with metal hydroxides have extensively been employed for removing dissolved organic substances (Saitoh *et al.*, 2017). However, coagulation technology enhances the removal of contaminants from sewage by adding high-dose coagulants to maintain a specific pH value (Luo *et al.*, 2019).

Adsorption is a competitive technology and significant in industrial effluents due to its ease of use, moderate experiment setting, minimal energy consumption, and

straightforward generation procedure (Sanakousar *et al.*, 2022; Feng *et al.*, 2022). Adsorbent-based technologies have proven to be one of the best ways to remove contaminants from water, as seen in Table 2.1 (Jin *et al.*, 2022). Developing high-adsorption capacity adsorbents with a rapid adsorption rate is the most important process (Sanakousar *et al.*, 2022; Feng *et al.*, 2022). However, the adsorption technique only affected the phase transfer of the contaminants, not their total removal (Sun *et al.*, 2022). The secondary pollutants must therefore be treated, which adds to the cost (Guo *et al.*, 2012).

Table 2.1: Examples of physical adsorption methods for the removal of OTC are reported in the literature.

Material	Equilibrium time (min)	Removal (%)	Ref.
Zn/Fe LDH	120	77.2	Zaher <i>et al.</i> (2020)
ZIF-8-Fe/Ni	240	92.6	Jin <i>et al.</i> (2022)
Halloysite nanoclay	90	62	Ramanayaka <i>et al.</i> (2020)
Magnetic MMT-biochor composite	480	98.9	Liang <i>et al.</i> (2019)
Cubic ZnO MOFs	60	99	El-Sewify <i>et al.</i> (2022)
Mag@ZnO-Co ₃ O ₄ composite	90	66.8	Lian <i>et al.</i> (2017)

2.2.2 Biological method

Biological methods (as seen in Table 2.2) use microorganisms to break down pollutant (Ahmad *et al.*, 2022; Kamarudin *et al.*, 2021) through biotransformation of different metabolic intermediates or by pure or mixed microbial culture through complete oxidation to CO₂ and H₂O (Oberoi *et al.*, 2019) in different conditions such

as aerobic, anoxic, and anaerobic (Zhu *et al.*, 2021). For instance, the biological wastewater treatment process is conventional activated sludge, sequencing batch reactor, and anaerobic digestion process (Zhu *et al.*, 2021).

The biological methods' inability to efficiently mineralise antibiotics, which have the potential to generate antibiotic resistance genes and bacteria, accumulates in organic form on the water bodies (Sun *et al.*, 2022; Yang *et al.*, 2018). Poor biodegradability of OTC necessitates pretreatment of some types of refractory organic matter prior to the biological treatment process (Zhang *et al.*, 2017). Additionally, a long treatment time is needed for antibiotic removal (Lu *et al.*, 2020).

Table 2.2: Examples of biological methods for the removal of OTC are reported in the literature.

Material	Time (days)	Removal (%)	Ref.
Microalgae-based technology	7	99	Wu <i>et al.</i> (2022)
Aerobic granular sludge sequencing batch reactor	33	88	Wang <i>et al.</i> (2019)
Acidic anaerobic digestion	14	60	Li <i>et al.</i> (2021)
Anaerobic ammonium oxidation	7	81.6	Shi <i>et al.</i> (2017)
Aerobic granular sludge	40	92.89	Li <i>et al.</i> (2020)
Strain <i>Ochrobactrum</i> sp	4	63.33	Shao <i>et al.</i> (2019)

2.2.3 Advanced oxidation processes (AOPs)

Antibiotics in the wastewater can be degraded or converted to tiny molecules using AOPs as a representative green method, which could reduce antibiotics' inhibitory impacts on bacteria and improve their biodegradability and elimination rate. Strong oxidation agents, such as hydroxyl ($\cdot\text{OH}$) and superoxide ($\cdot\text{O}_2^-$) are used in

AOPs to destroy pollutants (Wang & Zhuan, 2020; Kumar & Pal, 2018; Koutavarapu *et al.*, 2021). For the oxidation and mineralisation of organic molecules into carbon dioxide (CO₂), water (H₂O), and stable end products, ·OH is a potent oxidising agent (Kurt *et al.*, 2017; Moreira *et al.*, 2017). Typically, ·OH is yielded by reactions involving oxidants such as hydrogen peroxide (H₂O₂), ozone, or catalysts containing metal ions and semiconductors that are exposed to UV-Vis's irradiation or other energy sources (Perini *et al.*, 2018). The AOPs processes include homogeneous and heterogeneous photocatalytic oxidation.

When Fenton's reagent, which uses a mixture of H₂O₂ and Fe²⁺ salt, is subjected to UV light, it forms ·OH. This process is known as homogeneous photocatalytic oxidation (Pera-Titus *et al.*, 2004). This process needs to be carried out at a pH of about 3 to prevent iron precipitation. Nonetheless, since the common pH 6 or 7 condition is required in wastewater treatment, the increase in operational expenses related to acidification and base (Antonopoulou *et al.*, 2021). In addition, the iron sludge that forms as a result of the reaction should be eliminated, and a high concentration of Feⁿ⁺ is needed (Mirzaei *et al.*, 2017). As a result, these limitations pose a considerable barrier to the widespread adoption of homogeneous photocatalytic oxidation.

Photocatalytic oxidation using heterogeneous semiconductors could be the focus of AOPs for organic pollution elimination, including antibiotics. This technology is considered simple, economical, environmentally friendly and a non-toxic byproduct (Chen *et al.*, 2022) and, most importantly, organic pollutant can completely degrade into H₂O and CO₂ (Zhang *et al.*, 2022). Heterogeneous photocatalytic oxidation employs semiconductor oxides as a photocatalyst. The solid catalyst in the heterogeneous system can absorb organic contaminants in addition to

encouraging the production of active molecules in the system. Due to the interfacial effect, organic contaminants that have been adsorbed on a solid surface are more prone to decomposition (Wang *et al.*, 2022). The semiconductors or photocatalysts are metal oxides that are active under light irradiation and are non-toxic, cost effective in operation, and have a large surface area (Ayub *et al.*, 2020; Chong *et al.*, 2010).

Furthermore, it is necessary to assess how many variables, such as the photocatalyst dosage, pH, the initial concentration of pollutants, and ionic strength, affect the effectiveness of the removal process in a heterogeneous photocatalytic oxidation system over a range of time intervals. One of these crucial operational elements that greatly affects the characteristic of the photocatalyst is the solution's pH. Pirhashemi *et al.* (2018) and Du *et al.* (2022) highlighted that increasing the pH from 3 to 9 caused a slight decrease in OTC degradation from 91.2% to 82.5%. However, Li *et al.* (2022) discovered that raising the starting pH from 5 to 9 increased the rate of OTC removal from 56.2% to 90.5%. This improvement was due to the photocatalyst's surface having more OH⁻ ion, which facilitates the production of ·OH by photoinduced holes. Additionally, it is believed that the used oxidants lose their stability when the particles dissolve and produce the corresponding salts in excessively basic and acidic conditions (Pirhashemi *et al.*, 2018).

2.2.4 Basic mechanisms for AOPs

After a photocatalyst absorbs light, the photocatalytic oxidation reactions typically involve four main steps. The primary photocatalytic oxidation events are: (i) generation of the electron-hole charge carriers over the valence band (VB) and conduction band (CB); (ii) recombination of the photogenerated electron-hole (e⁻/h⁺) pairs; (iii) entrapment of the e⁻/h⁺ pairs in redox reactions; and (iv) oxidation of the

pollutant (Banerjee *et al.*, 2014; Panthi *et al.*, 2015). Photons having a wavelength equal to or larger than the band gap of a semiconductor, such as UV and visible light in the 360-600 nm range, irradiate the surface of the metal oxide in photocatalytic oxidation to generate e^-/h^+ pairs (Figure 2.2). The formation of e^- and h^+ is caused by the excitation of electrons from VB to the CB by the incidence of light, leaving holes in the VB. However, some of the photoinduced e^-/h^+ pairs go through a recombination process where they neutralise one another and generate heat. This is because the pairs are not energetically stable. The second stage significantly lowers the efficiency of the photocatalytic oxidation activity, whether on the surface or in the bulk (Ong *et al.*, 2016; Mamaghani *et al.*, 2017). In the third phase, the photoinduced holes and electrons move to the photocatalyst's surface and interact with the species that have been adsorbed there, creating a few species that can start a string of redox reactions (Pirhashemi *et al.*, 2018). For example, the hole in the VB reacts with water molecules to form $\cdot\text{OH}$, whereas the electrons in the CB react with dissolved oxygen species to form $\cdot\text{O}_2^-$. Finally, the reactive oxygen species (ROS) could oxidise and reduce pollutants molecules through photocatalytic oxidation processes, mineralising them completely into CO_2 and H_2O (Ponraj *et al.*, 2017). The following is a list of relevant reaction formulas in equations (2.1) - (2.4):

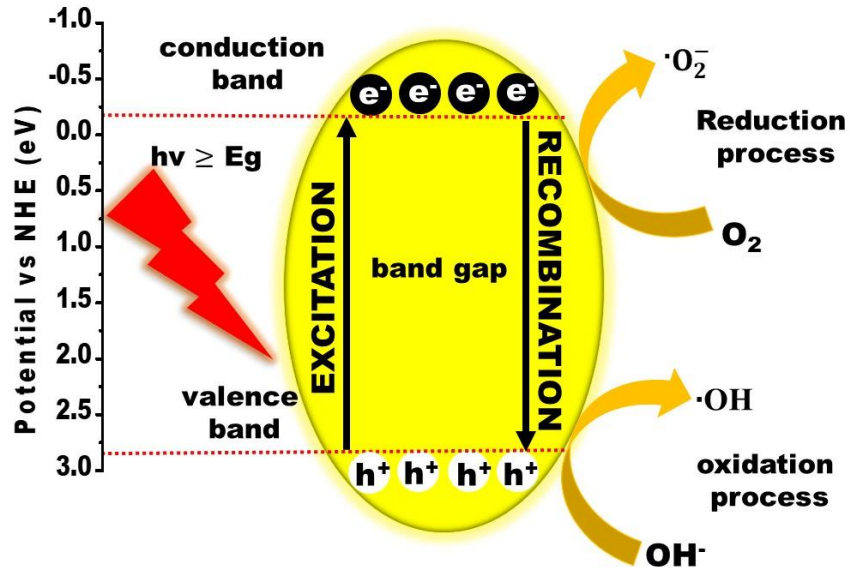
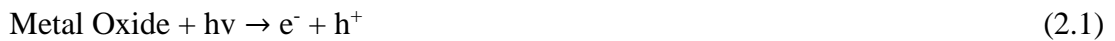


Figure 2.2: A schematic represents the general photocatalytic mechanism.



2.3 Metal oxide semiconductor as photocatalyst

Metal oxide nanoparticles (NPs) ability to create ROS in the presence of a suitable light source enables them to be used in a variety of applications (Türemen *et al.*, 2021). Metal oxide NPs have been exploited for photocatalytic oxidation applications because their band gap energies are sufficient for catalysis. Variations in the specific surface area of samples are simultaneously caused by changes in particles morphology and size (Cheng *et al.*, 2014). By adding additional active sites to its surface that are available for organic molecules to interact with, metal oxide can demonstrate a high surface-to-volume ratio at the nanoscale level, improving

photocatalytic oxidation efficacy in environmental remediation (Nunes *et al.*, 2021; Danish *et al.*, 2020). II-IV group semiconductors are composite materials made of IIB group metallic elements (Cd, Zn, Be, Mg, Ca and Sr) with group VI nonmetallic elements (O, S, Se and Te) (Zhang *et al.*, 2022). They have been examined due to their distinct functions when compared to other semiconductors, and they have been demonstrated to be photoactive in the near UV area (Wang *et al.*, 2017). Furthermore, this achievement can be attributed to their effectiveness in manufacturing nontoxic end products and ease of operation, as well as their good qualities such as environmental friendliness, biocompatibility, and low cost (Mohamed *et al.*, 2021). Metal oxides like nickel dioxide (NiO₂), titanium dioxide (TiO₂) (Guo *et al.*, 2021), zinc oxide (ZnO) (Nguyen *et al.*, 2022), tin (IV) oxide (SnO₂) (Nivetha *et al.*, 2022), zinc sulfide (ZnS) (Li *et al.*, 2022), cadmium sulfide (CdS) (Khan *et al.*, 2022), tungsten trioxide (WO₃) (Moghni *et al.*, 2022) and many more metal oxides have all been investigated as photocatalyst in the removal of antibiotics. Each of these semiconductors have unique, benefits, drawbacks, and restrictions.

Metal oxides like ZnO and TiO₂ are photocatalysts and have been suggested as a solution to all pollution concerns. ZnO is proven to be more effective compared to TiO₂ (Mittal *et al.*, 2014). ZnO is a category of n-type II-IV semiconductor (Sanakousar *et al.*, 2022) due to defects being present such as oxygen vacancies, zinc interstitials, and zinc antisites (Zhang *et al.*, 2022; Mahapatra *et al.*, 2022). It has significant lattice defects on the surface, making it an efficient photocatalyst material (Etacheri *et al.*, 2012). It has drawn a lot of interest as a potential metal oxide because of its superior properties such as non-toxicity, thermal stability, a large exciton binding energy (60 meV) (Sathish *et al.*, 2021; Dineshbabu *et al.*, 2022), affordability, a large number of active sites with strong surface reactivity (Suwanboon *et al.*, 2011; Li *et al.*,

2014), a broad band gap of 3.37 eV ($\lambda = 380$ nm) (Sanakousar *et al.*, 2022), chemical stability, a high initial activity rate, and the capacity to absorb a significant portion of the solar spectrum more effectively than TiO₂ (Ong *et al.*, 2018; Zhu *et al.*, 2020). Furthermore, the US FDA considers ZnO to be a “Generally Recognised As Safe” (GRAS) substance (Sathish *et al.*, 2021).

Even though ZnO has been widely used in photocatalytic oxidation, ZnO is only effective in absorbing photons in the UV region due to its high bandgap energy and suffers from a rapid recombination rate of electron and hole pairs (Ong *et al.*, 2018). Furthermore, since UV generates only 3-5% of the solar spectrum, photocatalytic oxidation applications necessitate the efficient utilisation of solar energy (Etacheri *et al.*, 2012). The optical absorption range of a semiconductor must be broadened and extended to include the visible-light region by narrowing the band gap to harvest the light energy efficiently (Abdullah *et al.*, 2022). Wide-bandgap semiconductors have thus been activated in a variety of ways to respond to visible light, including photosensitisation, heteroatom doping, charge transfer interaction, preparation of composite semiconductors, and modification with noble metals or rare earth metals. The enhancements can be more effectively realised with semiconductor NPs in addition to possessing a suitable band gap energy, as their tiny size allows for charge migration to reach the reaction site on the surface, reducing recombination (Medhi *et al.*, 2020). The size of the quantum dots was mostly responsible for the room temperature sensitivity (Das *et al.*, 2022). Additionally, adding quantum dots (QDs) is another creative way to enhance the photocatalytic oxidation activity when exposed to visible light (Paszkiwicz-Gawron *et al.*, 2021). It has been possible to change the physiochemical and optical properties of nanostructures since the photocatalytic oxidation activity is related to the band gap, adsorption ability, and electron-hole

separation, which are key factors determining the performance of photocatalytic materials (Liu *et al.*, 2020).

2.4 Semiconductor nanocrystals

Semiconductor nanocrystals are novel nanosized materials with a variety of advantageous features. Quantum rods (QRs), quantum dots (QDs), and quantum particles are some of the semiconductors it has designed (Abdel-Salam *et al.*, 2020). Furthermore, nanomaterials can be divided into zero-dimensional (0D) (quantum dots or primarily spherical nanoparticles), one-dimensional (1D) (nanowires, nanotubes, and nanobelts), two-dimensional (2D) (thin films and quantum wells), and three-dimensional (3D) (plates and flower-like) shapes (Tiwari *et al.*, 2012). In this study, QDs are highlighted due to their superb photo-physical properties, which are required to promote their photocatalytic oxidation applications. Brus, (1983) used the term ‘quantum dots’ for the first time to describe a three dimensionally restricted semiconductor quantum well and describe the characteristics of semiconductor QDs particles that demonstrate a quantum confinement regime by Weller, (1993). The QDs typically have a hierarchical structure that consists of a core semiconductor material encased inside a shell of another semiconductor and defined as an ‘almost spherical-shaped nano-sized substance’ (Azzazy *et al.*, 2007; Abdel-Salam *et al.*, 2020; Son *et al.*, 2022). A typical QDs has a diameter of 1-10 nm (Abdel-Salam *et al.*, 2020) and contains 10^3 to 10^6 atoms on average (Singh *et al.*, 2018; Cheng *et al.*, 2022). The QDs have become a major area of research because of their distinct size, dependent properties, and clearly defined electronic and optical properties (Chen & Bai, 2020).

2.4.1 Physicochemical properties of QDs

A type of NP that emits light is zero-dimensional semiconductor QDs (Borghei & Hosseinkhani, 2022). The QDs are size-tunable inorganic fluorophores with great light absorption and bright fluorescence, (Azzazy *et al.*, 2007; Borghei & Hosseinkhani, 2022). The colors they emit depend on their size, chemical structure, and surface coating, which can be simultaneously activated by a single UV light source (Abdel-Salam *et al.*, 2020; Son *et al.*, 2022). As shown in Figure 2.3, the fluorescence colour could be shifted from blue to green, yellow, orange, and red (Bruchez *et al.*, 1998; Tang *et al.*, 2010). Larger-sized QDs with diameters nearly 10 nm exhibit red or orange fluorescence at longer wavelengths with low intensity radiation. On the other hand, small-sized QDs at 1 nm emit light at shorter wavelengths and have green or blue emission with very high radiation strength (Abdel-Salam *et al.*, 2020).

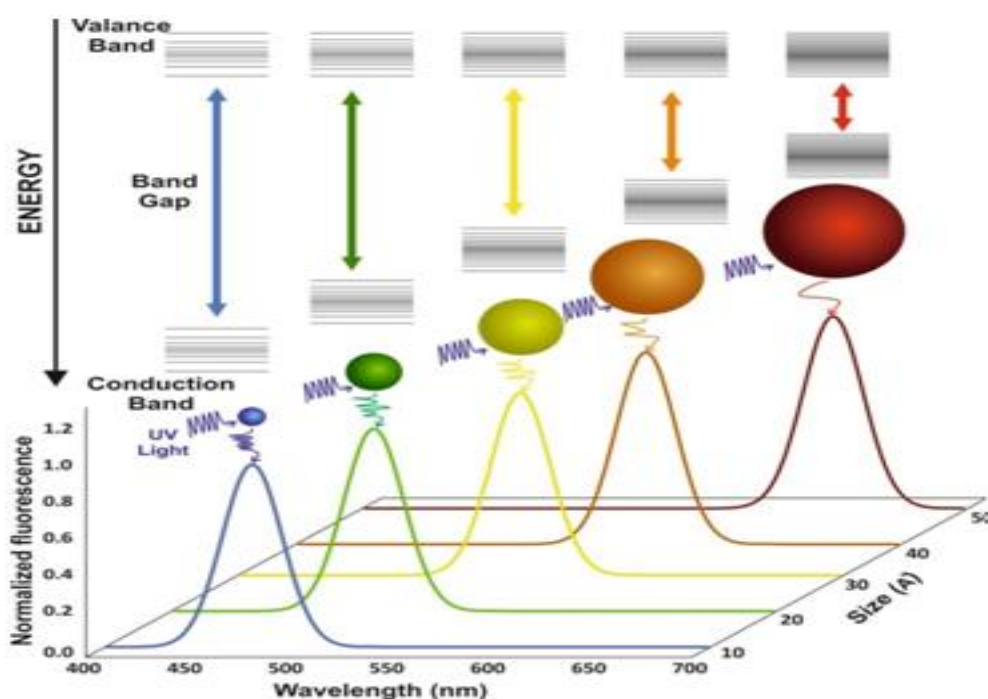


Figure 2.3: Emission and bandgap energy are based on particle size-dependent fluorescence color. Adapted from an article published by Samimi *et al.* (2017).

When incident light strikes the QDs, they absorb a photon with a higher energy than the band gap energies of the contributing semiconductor. The possibility of absorption at higher energies results in a broad absorption spectrum. A narrow symmetric energy band emission occurs when the exciton (electron-hole pairs) returns to a lower energy (Azzazy *et al.*, 2007). When a photon with energy greater than the QDs-band gap energy is absorbed, e^- are promoted from the VB to the CB, leaving an empty state “ (h^+) ” in the VB (Abdel-Salam *et al.*, 2020; Ilaiyaraja *et al.*, 2018). The e^- and h^+ then lose all of their energy and jump to the lower level of their CB and the upper level of their VB, respectively (Wegner & Hildebrandt, 2015). In bulk semiconductor material, e^- exists in a variety of different energy levels that are constant (Abdel-Salam *et al.*, 2020). However, at the nanoscale size to less than Bohr radius, the excitons will be confined in all three spatial dimensions and ultimately give rise to discrete quantum states (Bajorowicz *et al.*, 2018). Due to the limited mobility of e^- , more energy is required to stimulate the QDs to return their position to VB, resulting in a larger band gap energy being generated. This band gap energy can inhibit the recombination of photogenerated e^-/h^+ pairs, and energy is released (Bajorowicz *et al.*, 2018; Juzenas *et al.*, 2008). Fluorescence can be used to release energy via non-radiative decay (Ilaiyaraja *et al.*, 2018). Larger band gap energy in smaller QDs results in higher-energy photons being emitted, which correspond to a shorter wavelength, and vice versa (Maxwell *et al.*, 2020). Additionally, the QDs’ fluorescence emission normally varies from 450 to 850 nm, and the QDs can be tuned to emit at the appropriate wavelength based on their color even though QDs contain different sizes and compositions of QDs (Borghei & Hosseinkhani, 2022).

The photoluminescence (PL) of QDs contains two emission bands, one of which is UV, attributed to the exciton near the band edge, and the inception of a visible

(Vis) emission is ascribed to points of defect (Li *et al.*, 2016; Lin & Fu, 2001; Xu *et al.*, 2013). Examples of point defects are zinc vacancies (V_{Zn}) and zinc interstitials (V_{Zni}), which are primarily responsible for the blue emission. Green emission is caused by oxygen antisite (O_{Zn}) and oxygen vacancies (V_o). Lastly, oxygen interstitials (O_i) ought to be responsible for yellow or possibly orange-red emission (Li *et al.*, 2016; Ye, 2018). These defects are prevalent on the surface of QDs and play a significant role in the development of novel functionalities (Asok *et al.*, 2014). In accordance with Okeke *et al.* (2021), surface defects can enhance photocatalyst efficiency in order to slow down the rate at which photo-generated electron-hole pairs recombine. Electron-hole pair separation is made easier when holes are trapped in surface defects (Zhang *et al.*, 2014). Electrons can transfer to adsorbed sites through surface defects, which operate as charge carriers and traps and prevent the recombination of photoexcited electron-hole pairs (Kong *et al.*, 2022).

The nucleation and growth kinetics of QDs have a large influence on the concentration or density of these surface defects. Thus, precisely controlled reaction parameters are required for rapid nucleation and growth, which increase defect density and result in intense luminescence (Sarkar *et al.*, 2022). The defect density increases with decreasing QDs size owing to the higher surface-to-volume ratio (Asok *et al.*, 2014). Due to their nanoscale sizes, QDs always have a significantly higher number of surface atoms than their bulk counterpart (Zou *et al.*, 2018). In addition, the larger surface-area-to-volume ratio than their bulk counterparts allows for more photon absorption on the photocatalyst surface (Chen & Bai, 2020). Because QDs have a high surface-to-volume ratio, excitons in QDs can easily be trapped by surface defects and recombine non-radiatively, lowering UV emission efficiency (Chen *et al.*, 2022).

An overview of recently reported studies for the oxidation of antibiotic waste-based QDs photocatalyst is presented in Table 2.3. Since most electron-hole pairs in individual composite components quickly recombine, pure quantum dots or bare semiconductor NPs with a narrow band gap have minimal photocatalytic oxidation activity. Additionally, due to the large intrinsic band gap of QDs, UV light is the only source of their excitation. Thus, doping or loading can make up for these shortcomings. However, the response of a wide bandgap semiconductor to visible light can be controlled to improve its photocatalytic oxidation characteristics by combining it with a small bandgap semiconductor (Bajorowicz *et al.*, 2018). Additionally, the quantum size effect caused a large access of electrons and holes to the surface, resulting in efficient oxidation and reduction reactions. Last but not least, it is possible to create a high-area interface between the two semiconductors, which would improve the separation of photoinduced electrons and holes (Devi & Tharmaraj, 2019).

Table 2.3: List of recently reported studies on oxidation of antibiotics based on QDs.

Photocatalysts	Properties of QDs	Antibiotics	Light source	Percentage removal after modification	Percentage removal before modification	Reference
MoS ₂ /ZnO QDs	Particle size=7.5 nm	Tetracycline (20 mg L ⁻¹)	300 W Halogen lamp	95.6% after 80 min $k= 0.01 \text{ min}^{-1}$ Reusability = 5 cycle	Bare MoS ₂ =38.4% ZnO QDs= 25.6%	Chen <i>et al.</i> (2022)
ZnO QDs/TiO ₂ nanocomposite	Particle size=4.12 nm Band gap= 3.50 eV	Tetracycline (20 mg L ⁻¹)	48 W with two compact fluorescent lamp	98.0% after 60 min $k= 0.06807 \text{ min}^{-1}$ Reusability = 3 cycle	TiO ₂ NPs=32.4% ZnO QDs=68.8%	Iqbal <i>et al.</i> (2021)
BiVO ₄ /GQDs/PCN	Particle size= 5 nm Band gap=2.66 eV	Norfloxacin (20 mg L ⁻¹)	300 W Xe lamp ($\lambda > 420 \text{ nm}$)	86.3% after 120 min $k= 0.0148 \text{ min}^{-1}$ Reusability = 4 cycle	BVP/PCN=42.7% PCN=23.2% BiVO ₄ =37.1% g-C ₃ N ₄ =12.7%	Wang <i>et al.</i> (2021)
Floating ZnO QDs-Modified TiO ₂ /LLDPE Hybrid Polymer Film	Particle size= 4.12 nm Band gap= 3.50 nm	Tetracycline (40 mg L ⁻¹)	48 W with two compact fluorescent lamp	89.5% after 90 min $k= 0.01077 \text{ min}^{-1}$ Reusability = 8 cycle	TiO ₂ @LLPDE=42.7% ZnOQDs@LLPDE=53.4%	Iqbal <i>et al.</i> (2021)
NGQDs-BiOI/MnNb ₂ O ₆	Particle size= 5–10 nm	Tetracycline (10 mg L ⁻¹)	250 W Xe lamp ($\lambda > 420 \text{ nm}$)	87.2% after 60 min $k= 0.0331 \text{ min}^{-1}$ Reusability = 4 cycle	MnNb ₂ O ₆ = 7.2% BiOI= 30.5%	Yan <i>et al.</i> (2017)
p-n heterojunction CdS QDs/LaMnO ₃ composite	N/A	Oxytetracycline (40 mg L ⁻¹)	300 W high pressure Xe lamp ($\lambda > 420 \text{ nm}$)	70.0% after 60 min $k= 0.01736 \text{ min}^{-1}$ Reusability = 4 cycle	LaMnO ₃ =43.0% CdS QDs = 27.0%	Zhang <i>et al.</i> (2022)
CdS-Bi 1D-0D heterostructure	N/A	Tetracycline (20 mg L ⁻¹)	150 W Xe lamp	90.0% after 60 min $k= 0.034 \text{ min}^{-1}$ Reusability = 5 cycle	CdS = 52.0%	Chava <i>et al.</i> (2022)